Vertical Flight Society's Design-Build-Vertical Flight Competition Final Technical Report Submission

AUBURN

UNIVERSITY

Anthony M. Comer	Captain, Graduate Student
Stefanus H. Putra	Co-Captain, Graduate Student
Rajan Bhandari	Graduate Student
Imon Chakraborty, Ph.D.	Faculty Advisor

Vehicle Systems, Dynamics, and Design Laboratory (VSDDL)
Department of Aerospace Engineering
Auburn University

8 May, 2022

I. Executive Summary

The Vehicle System Dynamics and Design Laboratory (VSDDL) is a research lab within the Department of Aerospace Engineering at Auburn University that was established in August 2018. The lab's research focuses on aircraft systems, dynamics, control, and flight simulation, with the ultimate goal of incorporating these aspects into aircraft sizing and design. The current research and development pipeline at VSDDL consists of four sections: **(i)** vehicle sizing, performance analysis, and optimization, **(ii)** flight control system architecture design and optimization, **(iii)** flight simulation model development and piloted simulations, and **(iv)** subscale prototype development and piloted flight tests. This work aims to incorporate the fourth component of the lab's research vision (as shown in Figure 1) intended for next-generation aircraft concepts (mostly Urban Air Mobility (UAM)). The objective of this work is to develop a subscale model of the VSDDL LPC-03 Pheonix lift-plus-cruise UAM concept [1] and conduct subscale flight tests. If successful, this will provide confidence in the lab's development of Simplified Vehicle Operations (SVO) for UAM. The goal is to design an aircraft that meets the Request for Proposal (RFP) requirements while validating the control laws [2] that have been tested in flight simulators [3].

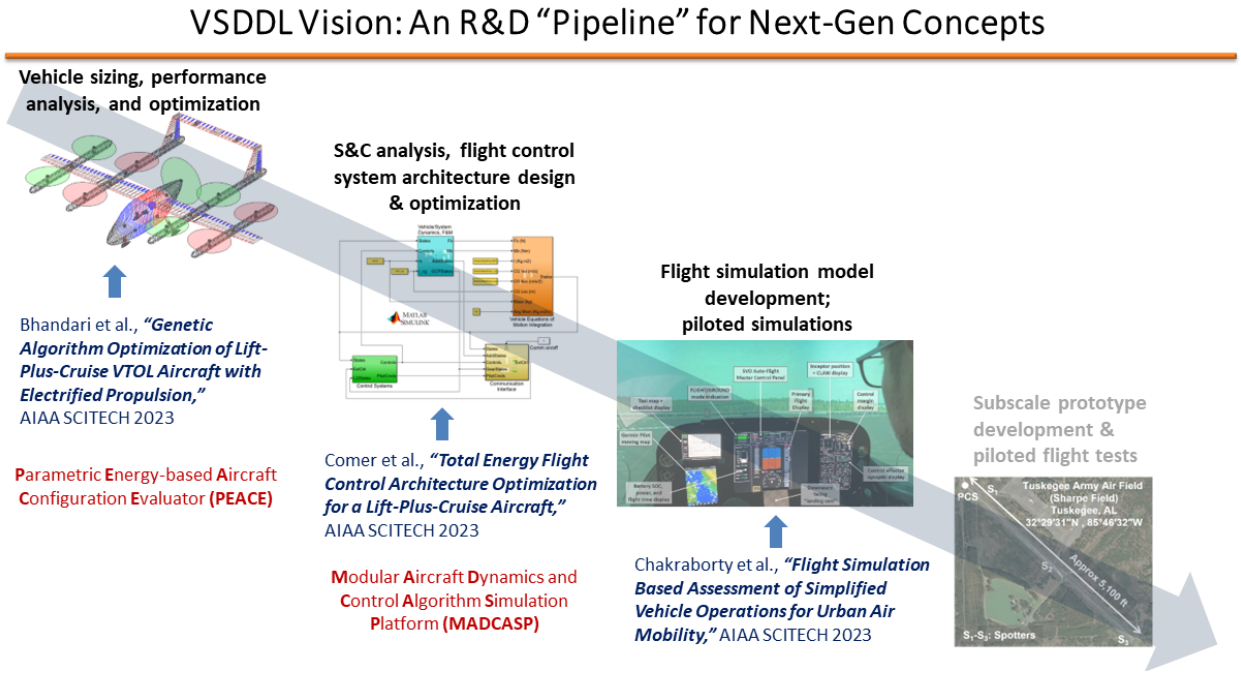

Fig. 1 VSDDL R&D "Pipeline" for next-gen concepts

The objective of this project is to develop a subscale version of the LPC-03 Phoenix aircraft (named LPC-Lite) that is capable of stable flight throughout the entire flight envelope using previously simulated flight control laws. The subscale model is limited to a maximum takeoff weight (MTOW) of 20 lbs while including a payload of at least 2 pounds. Additionally, the aircraft should **(i)** be no larger than 10 feet in any dimension, **(ii)** be equipped with a shunt plug in the appropriate location to control the power system, **(iii)** have a separate power source for the flight control system, and **(iv)** comply with the transmission frequency regulations specified by the U.S. Federal Communications Commission (FCC) Part 15 rules and International Telecommunication Union (ITU) Region 2 frequency allocations. These requirements are necessary to ensure the safe and successful flight of the aircraft.

The team performed an initial design trade study before down-selecting the final design configuration. The tilt-wing configuration was also considered as an alternative but ultimately rejected due to its mechanical and aero-propulsive complexity when compared to the lift-plus-cruise configuration. The final configuration featuring eight lift rotors and one cruise propeller was selected. The eight-rotor configuration features redundancy on off-nominal conditions such as rotor failure. Furthermore, this concept has already been tested by VSDDL in piloted flight simulations [3], but a physical prototype has never been tested at VSDDL until now. Prototypes of the final selected configuration have been made, and a trade study of sub-system configurations was done based on the aircraft mass and fabrication methods.

Preliminary sizing was done using the aircraft sizing tool, Parametric Energy-based Aircraft Configuration Evaluator

(PEACE), developed at VSDDL. Following the sizing campaign, fabrication began towards the end of February 2023. The propulsion and power system components were selected based on the results from PEACE. A table of viable motors, along with their maximum power and corresponding weight were used within PEACE to select motors. Batteries were selected based on the resulting energy weight requirements from PEACE. Before this sizing campaign, weight build-up relations for 3D printed parts were not available and had to be made (this method is elaborated further in Sec. VI).

Multiple iterations of the LPC-Lite were fabricated, and the weight build-up equations were improved with consecutive fabrications by weighing and updating the weight build-up equations. The propulsion system and power components also changed as the iterations progressed to meet the demands of the newly sized vehicles. The computer-aided design (CAD) model of the aircraft was consistently modified to better optimize components and increase manufacturing efficiency. Over a 20-day span, various indoor and outdoor flight tests were performed on the vehicles. The testing included hover and low-speed transition flight. Higher-speed flight is scheduled in the coming weeks along with autonomous flight testing. Leading up to the fly-off, the team will continue to improve the design and ensure that the vehicle conforms to the requirements of the competition.

II. Management Summary

The project timeline is shown as a Gantt chart in Figure 2. The VSSDL team consists of three graduate students and a faculty advisor from the aerospace engineering department at Auburn University. The faculty advisor is Dr. Imon Chakraborty, and he has guided the team throughout the project duration. The team captain is Anthony Comer, and the remainder of the team breakdown is shown in Table 1.

ID	Task Name	Duration	Start	Finish
1	**Aircraft Sizing (Baseline)**	**55 days**	**Sat 10/1/22**	**Thu 12/15/22**
2	**Aircraft Sizing and control model implementation, Version 1 (V1) detailed**	**51 days**	**Fri 12/16/22**	**Fri 2/24/23**
3	Aerodynamic Analysis	12 days	Fri 12/16/22	Sat 12/31/22
4	Complete Sizing	31 days	Mon 1/2/23	Mon 2/13/23
5	Flight Simulation	9 days	Tue 2/14/23	Fri 2/24/23
6	**Fabrication of V1**	**22 days**	**Mon 2/27/23**	**Tue 3/28/23**
7	**Indoor testing of V1**	**20 days**	**Sun 3/26/23**	**Thu 4/20/23**
8	**Resizing and weight calibration for V2**	**2 days**	**Fri 4/21/23**	**Sat 4/22/23**
9	**Fabrication of V2**	**2 days**	**Mon 4/24/23**	**Tue 4/25/23**
10	**Indoor Testing of V2**	**2 days**	**Wed 4/26/23**	**Thu 4/27/23**
11	**Outdoor Testing of V2**	**7 days?**	**Fri 4/28/23**	**Sat 5/6/23**
12	Hover flight test	2 days	Fri 4/28/23	Sat 4/29/23
13	Transition and forward flight test	6 days	Mon 5/1/23	Sat 5/6/23
14	**Design and Sizing of V3**	**4 days**	**Tue 5/9/23**	**Fri 5/12/23**
15	**Indoor and Outdoor Testing of V3**	**14 days**	**Sat 5/13/23**	**Wed 5/31/23**
16	**3d printing and assembly**	**68 days**	**Mon 2/27/23**	**Wed 5/31/23**
17	**Autopilot flight test**	**12 days**	**Mon 5/15/23**	**Tue 5/30/23**
18	**Improvements and changes**	**4 days**	**Wed 5/31/23**	**Sat 6/3/23**
19	**Fly-off**	**3 days**	**Tue 6/6/23**	**Thu 6/8/23**

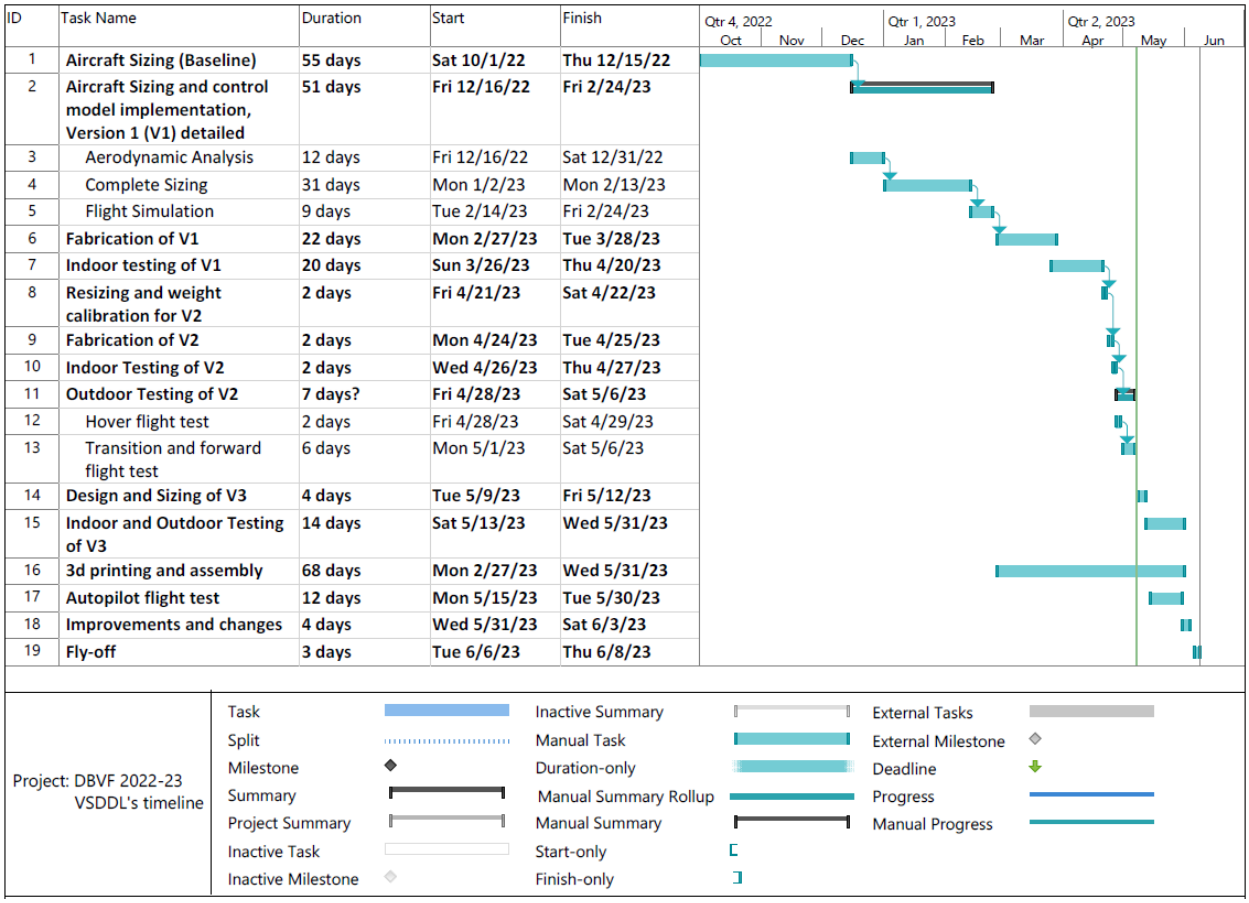

Fig. 2 VSDDL's DBVF 2022-2023 project timeline

The work allocation between team members is as follows:

- **Vehicle sizing and performance analysis:** Rajan Bhandari

- **Aerodynamics:** Rajan Bhandari
- **Hardware selection:** Rajan Bhandari and Anthony Comer
- **Vehicle CAD modeling:** Stefanus Putra and Anthony Comer
- **Hardware interfacing:** Anthony Comer
- **Flight control system design:** Anthony Comer
- **Flight simulation model development:** Anthony Comer
- **3D printing:** Anthony Comer and Stefanus Putra
- **Vehicle fabrication and testing:** Anthony Comer, Stefanus Putra, and Rajan Bhandari

Table 1 Team Roster

Name	Email	Class Standing	Role
Anthony M. Comer	amc0121@auburn.edu	Graduate Student	Captain
Stefanus H. Putra	shp0017@auburn.edu	Graduate Student	Co-Captain
Rajan Bhandari	rzb0109@auburn.edu	Graduate Student	–
Imon Chakraborty, Ph.D.	izc0018@auburn.edu	–	Faculty Advisor

III. Design Trade Studies

The fly-off consists of both vertical flight and forward flight portions. Therefore, the vehicle must transition between these flight modes throughout the mission. The LPC configuration allows for a simple transition due to the presence of orthogonal thrust sources. In the transition from VFM to FFM, the deck levels out as the cruise propulsor becomes active. As the aircraft increases speed, the lift generated from the wings increases, resulting in a natural decrease in the lift propulsor RPMs. Eventually, the aircraft reaches a transition speed where the vehicle can fly in forward flight mode, at which point the lift propulsors shut down completely. The transition from FFM to VFM occurs in a similar but opposite manner. The aircraft begins to slow, at which point the lift propulsors begin to turn back on in preparation for the vehicle's loss of lift from the wings. As the lift propulsors continue to spool up, the aircraft continues to slow down and eventually transitions back to rotor-borne flight. Finally, the aircraft continues to slow as the cruise propulsor shuts off, reverting back to helicopter-type control in VFM.

There are pros and cons to the different configurations. The LPC configuration provides more efficient lift during vertical takeoff and landing because of the multiple lift rotors optimized for vertical lift with cruise propulsors optimized for forward flight. However, during forward flight, the lift propulsors add unused weight to the vehicle, resulting in a heavier vehicle. Also, the stopped lift rotors add drag during forward flight. In a tilt-wing and tilt-rotor configuration, the same rotors must serve both vertical and horizontal flight modes, which can compromise the rotor's efficiency during one of the flight modes. Tilt-rotor and tilt-wing vehicles require more complex mechanical systems to account for the large structures that have to rotate, adding weight to the vehicle. This can also increase maintenance requirements in case of a sub-system failure along with aero-propulsive compexity. On the other hand, an LPC is more straightforward in terms of mechanical complexity due to the fixed wings and rotors. With this being the team's first competition and subscale model, structural simplicity was a major driving factor. Furthermore, the LPC-03 Phoenix has undergone extensive flight simulation and control law development and it was determined that the flight control system for an LPC provided the most straightforward approach for implementing a safe, robust flight control system in the vehicle. Due to these reasons, the team decided to down-select the LPC vehicle configuration.

There are several possible configurations for an LPC aircraft. Typically, it is logical to balance the rotors across the body axes of the vehicle (such as a quad-rotor, hexa-rotor, or octa-rotor). Each of these designs comes with pros and cons depending on the vehicle application. A quad-rotor configuration for an LPC lacks proper redundancy as it cannot continue stable flight following the loss of a single rotor. Therefore, a hexa-rotor and octa-rotor configuration must be compared. When considering a two-rotor loss, the remaining rotors must bear the additional disc loading associated with this loss. The power required to hover increases with a hexa-rotor configuration by a factor of 1.5 in the event of a dual-rotor loss. However, in an octa-rotor configuration, this factor is reduced to 1.33. Also, a hexa-rotor configuration for an LPC would require a rotor on the wing itself for symmetry. Otherwise, it would require three structural booms, further impeding the flow to the wings. The LPC-03 Phoenix design was more sensible in the structural design, featuring two longitudinal booms along each wing. Due to these considerations, an octa-rotor configuration was selected.

IV. Technical Innovation

The aircraft sizing framework PEACE was developed at VSDDL and was used to size this aircraft [1, 4, 5]. PEACE was orginally developed to study full-scale aircraft and that it was adapted during this project for sizing an Unmanned Aerial Vehicle (UAV). This tool is capable of designing and sizing both novel and conventional aircraft configurations. This framework employs a generalized, energy-based formulation of flight vehicle performance, not limited to conventional fixed or rotary-wing designs. The generalization of propulsive power and energy concepts enables equivalent sizing and analysis for conventional and electrified propulsion architectures. The aircraft is not considered a point mass; the rotational degrees of freedom are considered by trimming the aircraft model to calculate the power required or the available performance. This framework employs a parametric geometry representation of the aircraft and a set of resizing rules that govern the recalculation of component locations and dimensions over successive sizing iterations. The overview of aircraft sizing and mission analysis using PEACE is shown in Figure 3.

To analyze the aerodynamics of the aircraft, a strip theory-based model is used where all the lifting surfaces are broken down into spanwise strips, and then the loads on all the strips are evaluated and summed to give the net effect of all the lifting surfaces on the aircraft. The strip sectional aerodynamics are generated using FlightStream®. For non-lifting surfaces, lookup tables are used to characterize the loads developed on the non-lifting bodies such as the fuselage and booms. The propulsors are modeled using a blade element momentum theory model and a Pitt-Peters dynamic model using QMIL [6] and QPROP [7].

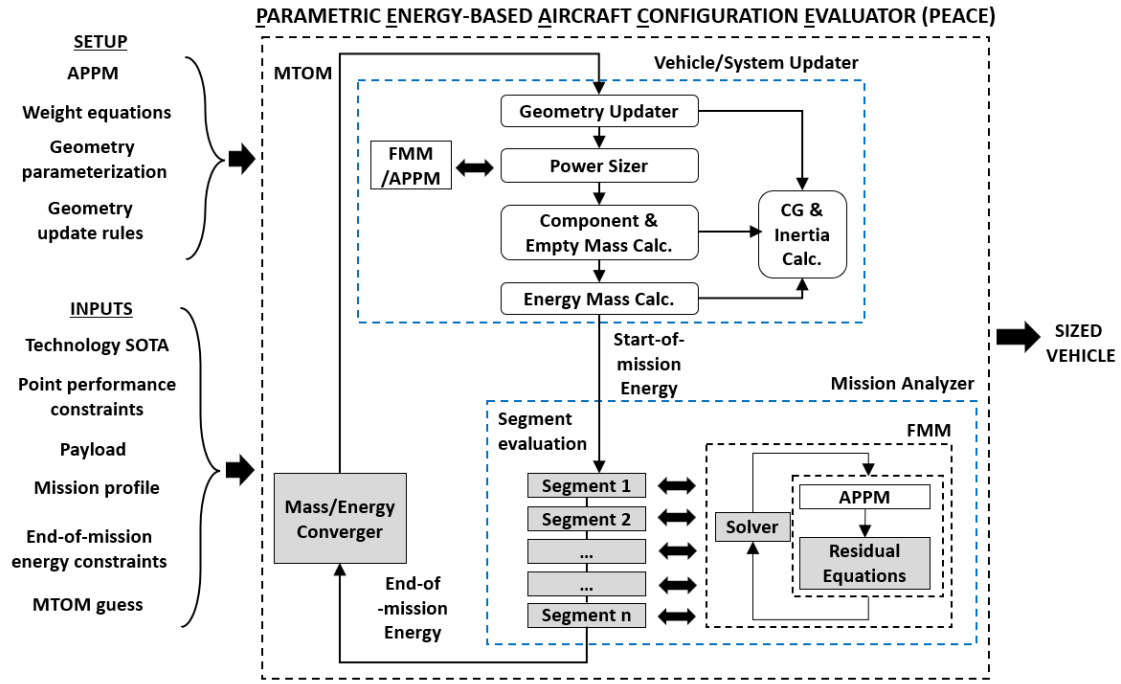

Fig. 3 Overview of PEACE aircraft sizing and mission analysis framework [1]

The propulsion system architecture of LPC-Lite is shown in Figure 4. There are a total of eight lift propulsors (LP) and one cruise propulsor (CP). Each propulsor is driven by an electric motor. The lift propulsors are mounted on inboard and outboard booms that are fixed on the wings. Each wing has an inboard flaperon (inboard of the inboard boom) and an outboard flaperon (between the inboard and outboard booms). Twin vertical stabilizers, each containing a rudder are mounted on the aft end of the inboard booms. A single horizontal stabilizer containing a large elevator panel is mounted on top of the vertical tails. The flaperons, elevators, and rudders are used to control roll, pitch, and yaw, respectively, in FFM. In VFM, roll is controlled using differential thrust between the left-side and right-side lift propulsors. Pitch is controlled through differential thrust between the fore and aft lift propulsors. The lift-propulsor axes are canted inboard or outboard, as shown in Figure 4, to generate yawing moments from the lateral thrust components. The yawing moment generated for each lift propulsor is in the same direction as its aerodynamic reaction torque. Yaw is controlled by increasing thrust on all lift propulsors that create a yawing moment in the desired direction while reducing

thrust on the remaining.

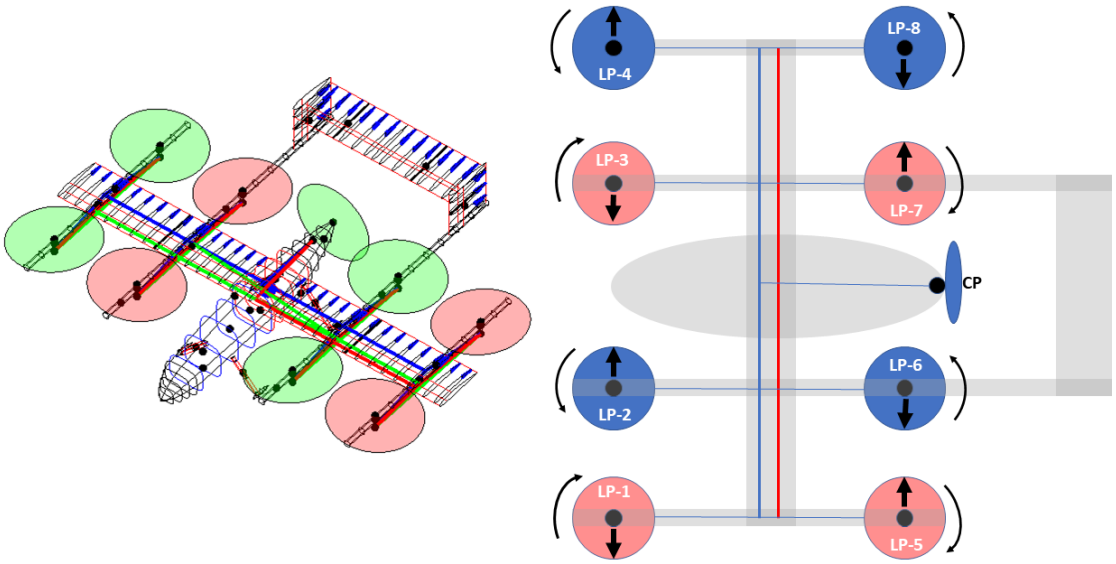

Fig. 4 LPC-Lite configuration overview and propulsion system architecture

The lift propulsor was designed using QMIL for a hover disk loading of 12.1 kg/m^2 (2.48 lb/ft^2) (assuming MTOW of 9 kg (19.84 lb) and a rotor diameter of 12 in. This was then verified using QPROP to determine whether it could generate additional thrust for off-nominal cases such as rotor failures. This process yielded the blade pitch and chord distributions as a function of normalized blade radius. These were then incorporated into PEACE to give the isolated lift propeller loads for axial and edgewise flow conditions. The interference between lift propulsors and the booms beneath them was modeled as a reduction factor for the net thrust. For the cruise propeller, QMIL was used to determine the propeller blade chord and twist distributions. The tables with nondimensional thrust coefficient and torque coefficient as a function of rpm were generated after verifying for off-nominal conditions using QPROP. These tables were incorporated into PEACE and queried during its evaluation. A set of lookup tables were created from the available market motors that were queried during power component sizing. The motors with a rated power more than the required power calculated using PEACE were selected.

The battery mass was estimated based on the energy required for the mission and the peak power requirement during the vertical climb. Specific power and specific energy were used to evaluate the energy mass required to support peak power and total energy, respectively. The battery mass is then estimated as:

$$m_{batt} = max\left(\frac{E_{req}}{(E/M)_{batt}}, \frac{P_{peak}}{(P/M)_{batt}}\right) \tag{1}$$

In equation 1, E_{req} is the total energy required to complete the design mission, and P_{peak} is the peak power that the battery has to supply for a short interval of time.

The horizontal and vertical stabilizers are sized using the tail volume ratio of the aircraft, which is 1.2 for LPC-Lite. The wing reference length for the horizontal tail volume ratio is chosen as its mean aerodynamic chord, while the wingspan is used as the reference length for the vertical tail volume ratio. The planform area of the horizontal stabilizer is calculated using the horizontal tail volume ratio. The planform area, when divided by the span of the horizontal stabilizer (the distance between two inboard booms), gives a constant chord. The tip chord of the vertical stabilizer and the constant chord of the horizontal stabilizer are equal. The tip chord and the vertical stabilizer's planform area are used to evaluate the span. The boom thickness was evaluated based on available carbon fiber materials.

A. Geometry Resizing

The wing reference area is calculated based on the wing loading and the MTOW in the current sizing iteration. The aspect ratio, taper ratio, and sweep remain constant. The 50% chord location of the wing root (projected to the

centerline) remains fixed at the origin of the geometry coordinate axes. The locations of lift propulsors are set such that the arcs of the inboard and outboard lift propulsors and cruise propulsors do not intersect. It is also ensured that the arcs of the lift propulsors are clear of the tip of the leading and trailing edges of the wings. During sizing, the positions of lift propulsors are adjusted such that the center of lift is positioned at the origin of the geometry coordinate system. The fuselage comprises four sections: nose cone, front cabin, aft cabin, and tail cone. Components such as the batteries, Pixhawk, GPS, FPV (First Person View) camera batteries, cruise motor and ESC, and landing gear are located within the fuselage. The target CG of the vehicle is the origin of the geometry coordinate system. This ensures balanced thrust across all lift propulsors in nominal hover conditions, minimizing the hover power requirements. To achieve this, all the component locations outside the fuselage are held constant, and the fuselage is moved fore or aft to shift the vehicle CG to the center.

B. Power Sizing

The power sizing module evaluates the power flow relationships at specified nominal and off-nominal conditions. More information regarding the design of the vehicle power flow relations can be found in Chakraborty et al. [1]. Based on the constraining flight conditions, propulsion system architectures (including batteries and motors) are sized. The threshold speed between vertical flight mode (VFM) and forward flight mode (FFM) was evaluated as $V_{th} = \sqrt{(2/\rho_{SL})(W_{to}/S_w)(1/C_{L_{ref}})}$, where ρ_{SL} is the sea level density, W_{to}/S_w is the wing loading referred to MTOW, and with $C_{L_{ref}} = 0.8$. The point performance constraints used for power sizing are listed in Table 2. The propulsion system components are sized to at least hover in case of failure of one or two rotors to ensure redundancy. For case numbers 11 (Hover SL, LP-1, 8 inoperative), 12 (Hover SL, LP-2, 7 inoperative), 19 (Hover Hot, LP-1, 8 inoperative), and 20 (Hover Hot, LP-2, 7 inoperative), one of the batteries is assumed to be inoperative.

Table 2 Point performance constraints for power sizing

Case no.	Description	Flight Mode	Airspeed (KTAS)	Pressure altitude, ft	Density altitude, ft	ΔISA (°C)	FPM (ft/min)
1	Cruise	FFM	60	400	3000	23	0
2	Climb Sea Level	VFM	51	0	0	0	200
3	Climb Hot	VFM	53	400	3000	23	200
4	Hover	VFM	0	0	0	0	0
5	Vertical Climb	VFM	0	400	400	0	400
6	Hover SL, LP-1 INOP	VFM	0	0	0	0	100
7	Hover SL, LP-2 INOP	VFM	0	0	0	0	100
8	Hover SL, LP-5 INOP	VFM	0	0	0	0	100
9	Hover SL, LP-6 INOP	VFM	0	0	0	0	100
10	Hover SL, LP-1, 8 INOP	VFM	0	0	0	0	100
11	Hover SL, LP-2, 7 INOP	VFM	0	0	0	0	100
12	Hover Hot	VFM	0	400	3000	23	0
13	Vertical Climb Hot	VFM	0	400	3000	23	400
14	Hover Hot, LP-1 INOP	VFM	0	400	3000	23	100
15	Hover Hot, LP-2 INOP	VFM	0	400	3000	23	100
16	Hover Hot, LP-5 INOP	VFM	0	400	3000	23	100
17	Hover Hot, LP-6 INOP	VFM	0	400	3000	23	100
18	Hover Hot, LP-1, 8 INOP	VFM	0	400	3000	23	100
19	Hover Hot, LP-2, 7 INOP	VFM	0	400	3000	23	100

C. Flight Simulation Model Development

A flight simulation model of the LPC-Lite was created based on the sizing results from PEACE. The simulation model was developed using MATLAB/Simulink and VSDDL's *Modular Aircraft Dynamics and Simulation Platform* (MADCASP) framework. MADCASP allows for the vehicle to be trimmed at different flight conditions. These trim conditions were then used to generate linear time invariant models of the vehicle, allowing for flight control system development and tuning to occur. The flight simulation model features an identical flight control system architecture as the hardware version but with different sources for pilot inputs, sensor states, and parameters. The flight simulation model interfaces with third-party visualization software, such as X-Plane, and provides real-time simulation.

D. Flight Control System Design and Integration

The LPC-Lite features a total energy-based flight control system (FCS) architecture for a full-scale LPC aircraft and is shown in Figure 5. This FCS was designed, optimized, and simulation tested in a paper by Comer and Chakraborty [8]. The same FCS was used during a piloted simulation campaign involving the LPC-03 Phoenix [3]. For the LPC-Lite, the commands generated from the pilot inputs are as follows:

- $u_{lat}, \in [-1, +1]$ - commands a lateral velocity $VLAT_{cmd}$ in VFM and a direct bank angle ϕ_{cmd} in FFM
- $u_{lon}, \in [-1, +1]$ - commands a vertical velocity VV_{cmd} in VFM and FFM
- $u_{dir}, \in [-1, +1]$ - commands a yaw rate r_{cmd} in VFM based on pilot input, and auto-generates the yaw rate required for turn
- $u_{acc}, \in [-1, +1]$ - commands a normalized acceleration $\dot{V}/g_{cmd}$ in VFM and FFM

Moving left-to-right, the pilot inputs (coming from the transmitter) first pass through the *Inceptor to command mapping* subsystem. This subsystem is responsible for control command blending and command generation for the TECS and inner-loop controllers. A normalized acceleration command and vertical velocity command are generated in the longitudinal axis and are inputs to the *TECS core* subsystem. The Total Energy Control System (TECS) was first proposed in the 1980's by Lambregts [9–12] in an attempt to address some of the inherent deficiencies in single-input-single-output (SISO) autopilot systems. The outputs from this subsystem are thrust commands for the lift and cruise propulsors along with a pitch attitude command θ_{cmd}. Details regarding the generation of these commands can be found in [8]. This pitch attitude command, along with the generated bank angle command ϕ_{cmd} and yaw rate command r_{cmd} are inputs to the *Inner-loop LQI controllers* subsystem. The LQI controllers are of reduced order, and act to generate normalized lateral, longitudinal, and directional commands (u_{lat}, u_{lon}, and u_{dir}, respectively). These commands are realized from

$$\begin{aligned} u_{lon} &= -K_{long}^{1\times 3}\begin{bmatrix} q & \theta & \int e_\theta\, dt \end{bmatrix}^T \\ \begin{bmatrix} u_{lat} & u_{dir} \end{bmatrix}^T &= -K_{lat}^{2\times 5}\begin{bmatrix} p & r & \phi & \int e_\phi\, dt & \int e_r\, dt \end{bmatrix}^T \end{aligned} \tag{2}$$

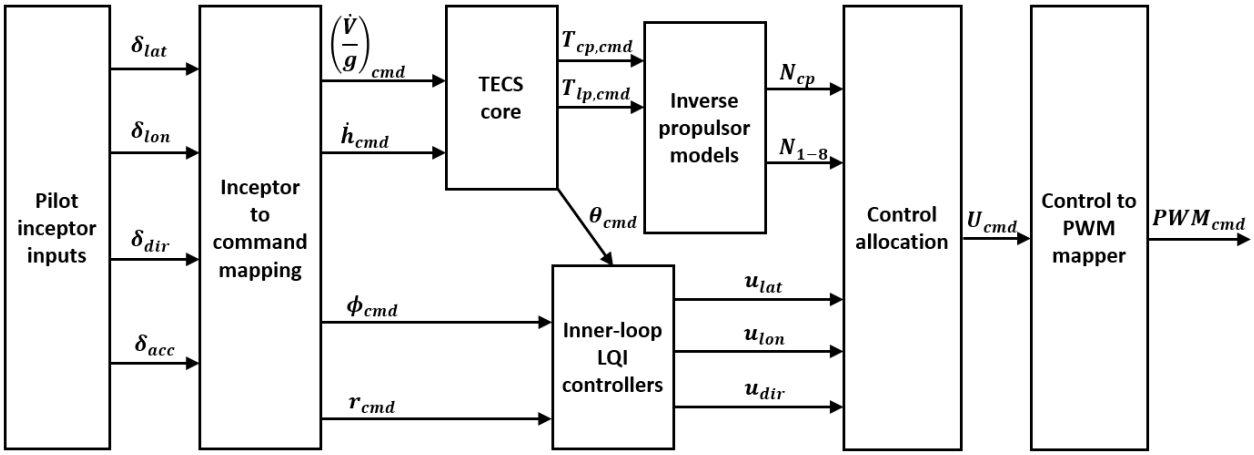

Fig. 5 LPC-Lite flight control system architecture

Where q is pitch rate, θ is pitch attitude, $\int e_\theta \, dt$ is integrated pitch command error, p is roll rate, r is yaw rate, ϕ is bank angle, $\int e_\phi \, dt$ is integrated bank command error, and $\int e_r \, dt$ is integrated yaw rate command error. The thrust commands generated from the *TECS core* subsystem then pass through the *Inverse propulsor models*. The inverse propulsor models are determined from the simulation model results and convert thrust commands into corresponding RPM commands for the lift and cruise propulsors. These five commands then feed directly into the *Control allocation* subsystem. This converts the five main command "groups" into control effector commands. The control effectors include flaperons, elevators, rudders, lift prop RPMs, and cruise prop RPM. Finally, the control effector commands feed into the *Control to PWM mapper* subsystem, which converts the incoming control effector commands into corresponding pulse width modulation (PWM) signals to be sent to the ESCs and servos. Before flight testing, the lift and cruise motor and propeller combination is thrust tested to generate a mapping of PWM to RPM. This is then used to quickly convert the incoming RPM command of each propulsor into an accurate PWM signal.

The flight control system is modeled using MATLAB/Simulink and is directly uploaded to the Pixhawk board using MATLAB's UAV Toolbox [13]. This toolbox allows for sensor data and transmitter inputs to be directly read into the model and generates PWM signals for the Pixhawk to send for controlling the vehicle. To allow live tuning, the internal firmware of the Pixhawk has been slightly modified, allowing custom parameters to be added within the Simulink model from the Pixhawk itself. These parameters can be viewed and changed from QGroundControl through a telemetry stream for live-tuning of FCS parameters. This has proven to be very useful for in-the-field, on-the-fly testing of different flight parameters. Changes made to the FCS architecture can be quickly realized by simply reuploading the model to the board from a laptop or desktop computer. Gain tuning has been done in the field while flying using this method, allowing for quick gain scheduling to occur.

V. Design Definition

A. Mission Profile

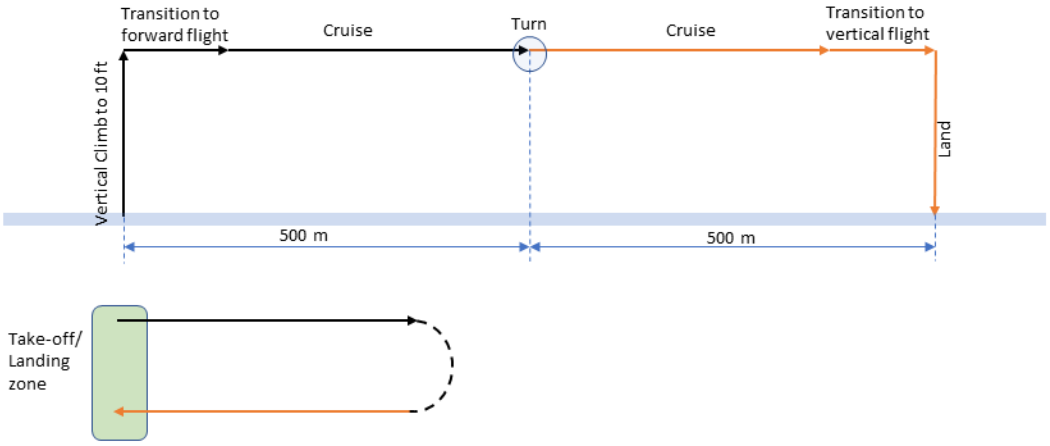

Fig. 6 Mission profile for one lap of flight performance and autonomy course

The mission profile for which the aircraft was sized is shown in Figure 6, which consists of a vertical climb to 10 ft, a transition to FFM, a cruising segment for 500 m followed by a turn, another 500 m cruise segment, a transition back to VFM, and a landing. The energy components were sized to provide power to complete six laps of manual flight. A payload of 2 lb would be carried by aircraft over the entire course of the six laps. The batteries connected in parallel were assumed to give power to the lift and cruise motors during VFM and FFM.

B. Design Revision

LPC-Lite version one was sized using PEACE. The weight build-up relations for 3D-printed parts were determined by 3D-printing representative wing sections with varying chord and span lengths. The varied pieces were then weighed to establish the weight of a 3D-printed aerodynamic surface as a function of the chord and span. Initial linear estimates underpredicted the true weight, so the weight build-up relations for 3D-printed aerodynamic surfaces were further tuned

with each iteration. The resulting weight increase from the improved 3D-printed part weight estimate required the lift motors to be upsized in the second version. The power cabling design was improved from the first iteration to reduce the clutter within the fuselage area. The new cabling design featured a main power rail passing through the entire wing, greatly reducing the wiring within the fuselage area. This also allowed for better space management of other key internal components (e.g., Pixhawk, batteries, etc.). TA general schematic of the power cabling architectures used in versions one and two are shown in Figure 7. The power cabling architecture in version two allows for a connection to be used from the main bus to the required shunt plug.

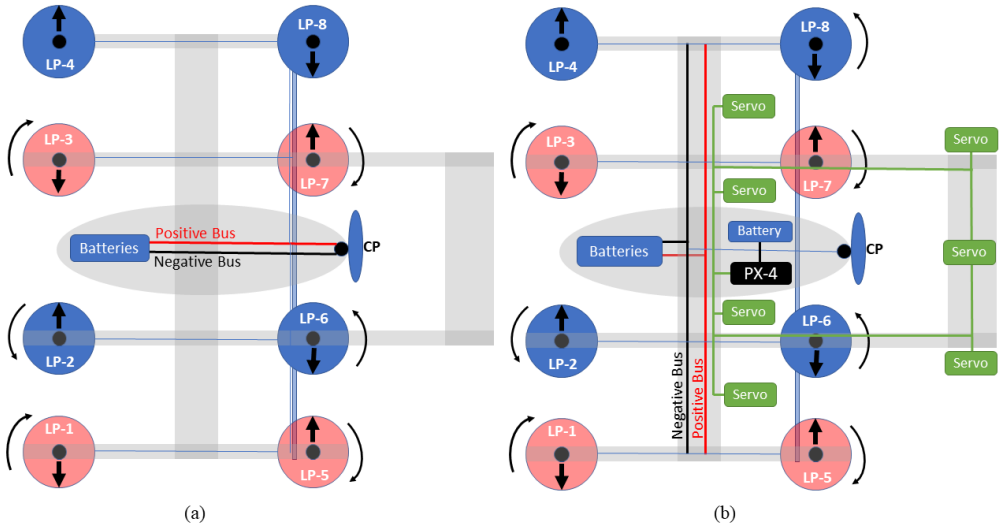

Fig. 7 Schematic of power cabling, (a) Version 1, (b) Version 2

Table 3 Weight build-up equations for aircraft components

S.N.	Component	Weight Equation	Remarks
1	Fuselage	$2.2\rho\pi\left((CG_x + 2l_{batt})(r+t)^2\right)$	CG_x = distance of battery CG from aircraft CG, l_{batt} = length of batteries, r = battery width + clearance, t = thickness of fuselage skin, and ρ is the density of material used
2	Wing	$2.96\left(1.88(b_w-3)+2.21(c_w-9)+40\right)$	b_w is the semi span, c_w is the root chord length (in inches)
3	Vertical Tail	$5.42\left(1.88(b-3)+2.21(c-9)+40\right)$	b is the span, c is the root chord length (in inches)
4	Horizontal Tail	$8.99\left(1.88(b-3)+2.21(c-9)+40\right)$	b is the span, c is the root chord length (in inches)

After building the second version and weighing the components, an underprediction was still present in the fuselage, wing, and tail. The weight build-up relations were once again improved within PEACE to obtain a more accurate weight estimate. The revised weight build-up relations for the fuselage, wing, and tail are shown in Table 3. Individual components, such as motors, propellers, and electronics, were weighed and recorded within PEACE. The weight breakdown of the structural components is listed in Table 4, and the compliance matrix of all the components are listed in Table 5.

C. Specification of components

The specifications of the current (subject to change) propulsion system, power system, flight controller, and other electronics are listed below:

1) **Lift motors and rotors**: The lift motors are "Cobra CM-2814/24", 700 Kv, and each motor weighs 129.8 g, including cabling. This motor, when operated with the APC 12x4.5-MR propeller, is able to produce a static

Table 4 Weight breakdown of LPC-Lite version 2

Component	Mass (g)	CG_x (in)	CG_y(in)	CG_z(in)	Weight Fraction (%)
Fuselage	1037	3.42	0	0.09	11.61
Wing	820	0.59	0	-1.74	9.18
Horizontal stabilizer	400	-23.20	0	-7.24	4.48
Vertical stabilizer	280	-23.20	0	-4.22	3.14
Booms	318	-4.78	0	-1.63	3.56
Landing gear	176	2.19	0	3.51	1.97
Structures	**3031**	**-3.68**	**0**	**-1.59**	**33.94**
Lift props	177	0	0	-2.26	1.98
Lift motors	1039	0	0	-1.63	11.63
Cruise prop	24	-12.74	0	-2.28	0.27
Cruise motor	271	-12.74	0	-2.26	3.03
Power cabling	880	0.61	-0.0296	-1.26	9.85
ESCs	634	-1.08	0	-0.51	7.10
Servo motors	255	-6.91	0	-2.01	2.86
Propulsion	**3250**	**-2.01**	**0**	**-1.42**	**36.39**
Avionics	**430**	**7.33**	**0**	**0.21**	**4.82**
Systems	**399**	**4.49**	**0**	**0.13**	**4.47**
Empty weight	**6810**	**-2.48**	**0**	**-1.42**	**76.26**
Batteries	**1210**	**12.57**	**0**	**1.39**	**13.55**
Payload	**910**	**-0.03**	**0**	**0.10**	**10.19**
Gross weight	**8930**	**-0.0009**	**-0.0023**	**-0.83**	**100.00**

thrust of 1.7 kg with a shaft power of 304 W. The motors are able to give a continuous peak power of 340 W when they operate using 4S Li-Po batteries with an input voltage of 14.8 V.

2) **Cruise motor and rotor**: The cruise motor is a "Cobra C-3525/12, 650 Kv", which weighs 271 g, including cabling. This motor, when operated with an APC 11x8.5-E propeller, is able to provide a static thrust of 2.3 kg with a motor shaft power of 673 W. This motor can provide a continuous peak power of 770 W and 1150 W when driven by 4S and 6S batteries, respectively.
3) **Batteries**: The two battery packs used are connected in parallel to provide common power to the lift and cruise motors. The "HOOVO 4S Lipo Battery" was selected for powering lift and cruise motors. A shunt plug will be installed between these two batteries that can quickly shut off the power to the propulsion system. Also, a fuse directly in-line with each battery's positive terminal will be connected with a current rating less than the maximum continuous discharge rating of the battery. The "iFlight Fullsend 650mah" battery was selected to independently power the flight control system. The FPV camera uses a separate power source supplied by a "HHZ 3000 mAh" rechargeable Lipo battery. The specifications of the batteries for all three applications are shown in Table 6.
4) **Avionics**: The "Pixhawk 1 APM 2.4.8, NEO-M8N, GPS 3DR, 915 Mhz Radio Telemetry Set" were used for flight control systems, GPS, and telemetry. The transmitter used for flight control transmission is the "RadioLink AT10", which operates at 2.4 GHz. The flight controls were implemented using MATLAB's "UAV Toolbox Support Package for PX4 Autopilots" in conjunction with QGroundControl for in-flight tuning [13]. MATLAB's support package allowed the team to implement our own flight control laws (further described in IV). The total weight of these components, with the exception of the transmitter, weighed a total of 310 g.

Table 5 Compliance matrix of all aircraft components

S.N.	Components	Requirements	Compliance
1	Fuselage	Maximum dimension ≤ 10 ft	Complied
2	Wing with control surfaces	Maximum dimension ≤ 10 ft	Complied
3	Tail with control surfaces	Maximum dimension ≤ 10 ft	Complied
4	Booms	Maximum dimension ≤ 10 ft	Complied
5	Landing gear	-	
6	Lift motors	Must be electrical	Complied
7	Lift rotors	-	
8	Cruise motor	Must be electrical	Complied
9	Cruise rotor	-	
10	Lift motor ESCs	-	
11	Cruise motor ESC	-	
12	Propulsion system batteries	Must be no more than 6S, and 100 Whr	Complied
13	Flight control system battery	Must be no more than 6S, and 100 Whr	Complied
14	FPV	Must operate on 902-928 MHz	Complied
15	Pixhawk	Must operate on 902-928 MHz	Complied
16	Transmitter and receiver	Must operate on 902-928 MHz	Complied
17	LIDAR and GPS	Must operate on 902-928 MHz	Complied
18	Power cabling	-	
19	Shunt plug	Must be red	Complied
20	Servo motors	-	
21	Payload	At least 2 lb	Complied
22	Miscellaneous	-	

Table 6 Propulsion, flight control, and FPV battery specifications

S.N.	Propulsion Battery	Flight Control Battery	FPV Battery
Name	HOOVO 4S Lipo Battery	iFlight Fullsend	HHZ Lipo Battery
Cells	4	4	2
Discharge Rating (C)	120	95	8
Capacity (mAh)	6200	650	3000
Capacity (Wh)	91.76	9.62	22.2
Mass (g)	522	78.5	65

D. Structure

The dimensions of the LPC-Lite V2 are shown in Figure 9. All of the structural components comply with the maximum allowable dimension of 10 ft, as stated within the RFP. The carbon fiber rods are used as spars in the wing, tail, and fuselage, and have a density of 0.056 lbs./cu. in. The LPC-Lite V2 was tested for its structural integrity by applying a 9 kg load on top of the CG of the aircraft, which is shown in Figure 8. The aircraft was supported at the tip of the wings to simulate a maximum root bending moment. A load of 9 kg was selected to simulate a 60-degree banked turn (the maximum allowable bank angle for this aircraft). The wings deflected by 1 cm, and the 9 kg load was applied for 10 minutes. A similar test was performed on the inboard booms to test longitudinal stiffness. The same 9 kg load was applied to the center of gravity, and the aircraft was supported on the tips of the inboard booms. The aircraft CG deflected by 0.7 cm, and the load was applied for 10 minutes. In both tests, the aircraft managed to return to its original

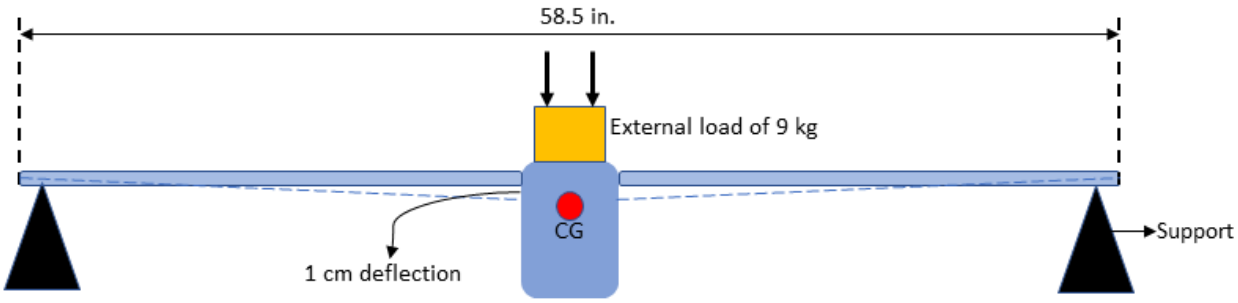

Fig. 8 Schematic of structural test of LPC-Lite V2

condition after testing, giving us confidence that the structural integrity is sufficient for the wings to handle a load two times its weight. Furthermore, initial flight testing of speeds around 30 mph has resulted in no visible structural degradation. The aircraft has also experienced multiple hard landings that were estimated to be well in excess of the maximum load factor expected to be experienced during flight.

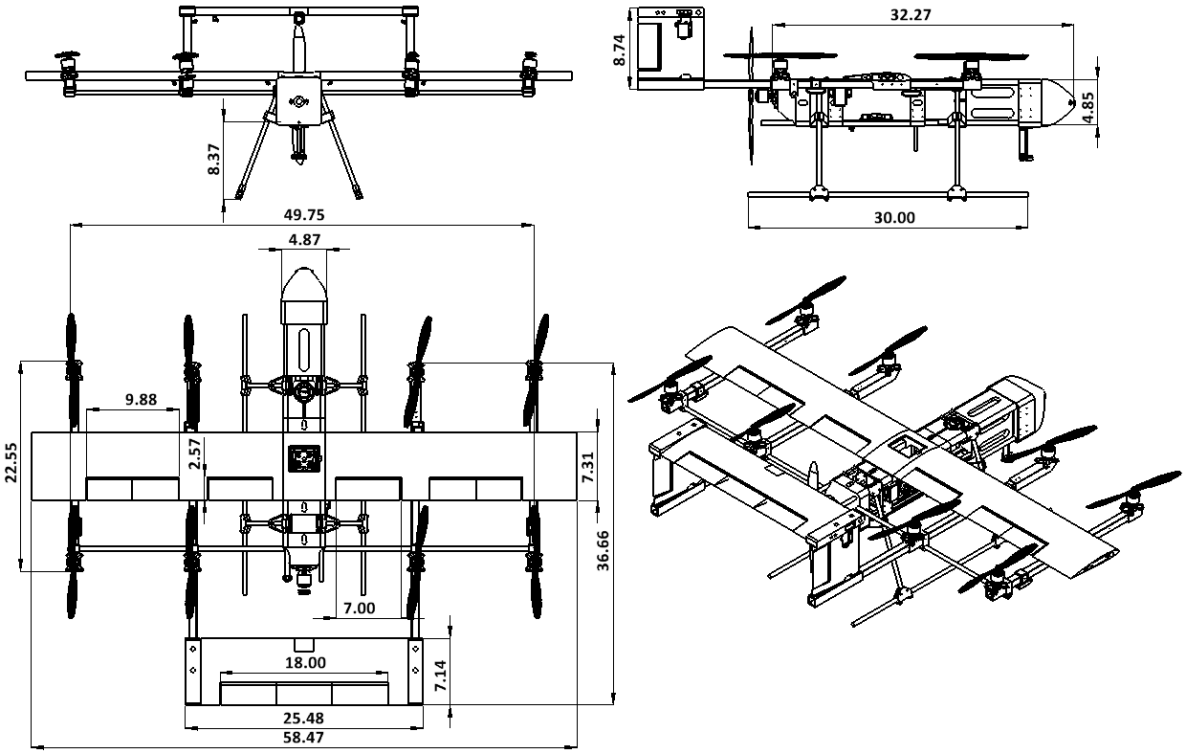

Fig. 9 CAD drawings of LPC-Lite V2

E. Aerodynamic Performance and Stability

The geometry of the bare airframe generated from PEACE (before sizing) was exported to FlightStream®, a surface vorticity solver (explained in section IV) to generate the sectional aerodynamic characteristics, namely, lift, drag, and pitching moments. A reduced order model (ROM) for downwash distribution was generated in FlightStream®. The ROM comprises coefficients for each strip of each lifting surface, moving from root to tip, that are used to compute the net circulation for each strip as a function of strip velocities and local angle of attack (AOA). The strip circulation distribution gives the strip downwash, and the strip-induced AOA is computed from the downwash and freestream velocity seen by the strips. The lift and drag on each strip were then queried using the effective AOA for each strip. The

effective AOA was computed by subtracting the induced AOA from the geometric AOA. The computed strip loads were then transferred from individual quarter-chord points to the aircraft moment reference center based on strip quarter-chord points to the aircraft moment reference. They were then summed to obtain net aerodynamic loads due to the lifting surfaces with respect to the aircraft moment reference center. The aerodynamic load contributions from non-strip components, such as the fuselage and booms, were computed using lookup tables comprising axial, lateral, and normal forces as well as rolling, pitching, and yawing moments for the components as functions of AOA and sideslip angle. The lift-to-drag ratio (L/D) predicted by FlightStream®was around 11 when the drag due to lift rotors in FFM was not predicted. FlightStream®also did not account for miscellaneous components used during flight such as landing gear, motors, and other small items. A conservative estimate of the L/D for the LPC-Lite V2 was around 5 when including all items on the aircraft.

The static stability of the aircraft was also evaluated using FlightStream®. The moment coefficient about the body-fixed y-axis was calculated for different points along the body-fixed x-axis in the vicinity of the CG of the aircraft. The neutral point of the aircraft was found to be aft of the CG by 3.2 inches, meaning that the aircraft was statically stable.

The open-loop dynamic stability was determined from the simulation model. The aircraft was dynamically unstable in VFM (as is expected of rotary-wing vehicles), gradually becoming stable as the airspeed increased. The LPC-Lite V2 features an integrated fly-by-wire flight control law that ensures dynamic stability throughout the entire flight regime. Initial gain values were determined from a gain optimization campaign. The details regarding this optimization process can be found in [8]. The usefulness of these gains was tested in single-axis hover tests by verifying the stability of the gains from the simulation model. This process is described further in Section VII. The robustness of these gains was tested by performing flight tests at speeds up to 30 mph, where the vehicle remained dynamically stable.

The predicted range for the aircraft while cruising at 60 kts is 6000 m equating to six laps of the design mission. This range was predicted with the aircraft carrying 2 lb of payload over the entire mission. The total predicted endurance time of LPC-Lite V2 is around 7.8 minutes.

VI. Fabrication Methods

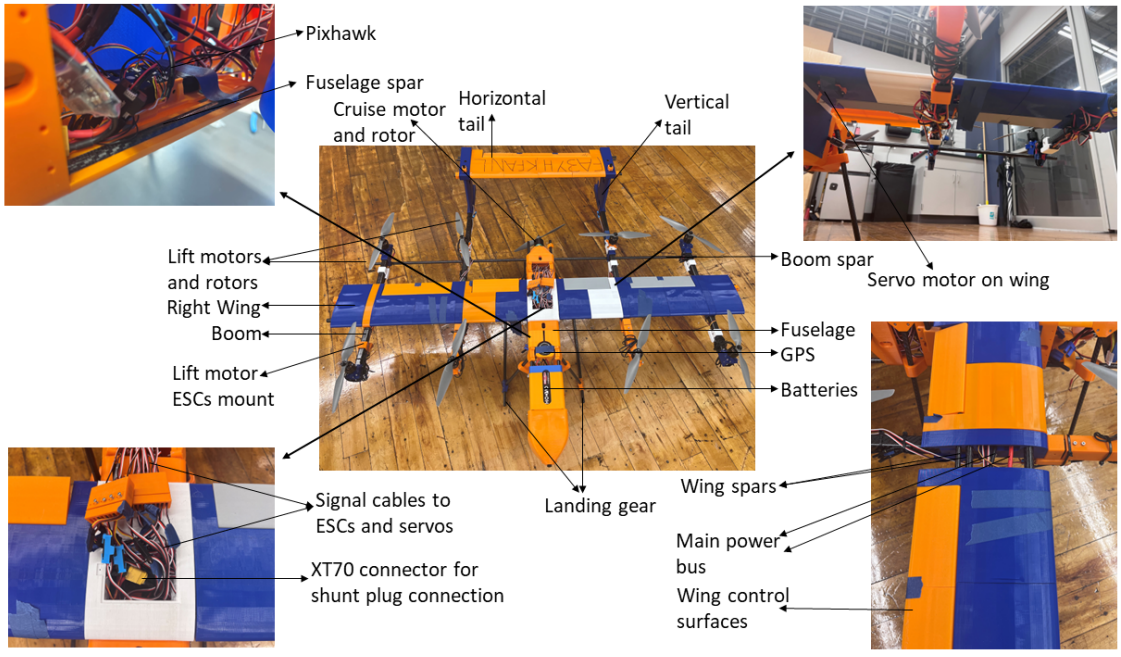

Fig. 10 Structural layout and components of LPC-Lite V2

LPC-Lite V2 components were either bought off-the-shelf or manufactured in-house. Structural components such as the wing and tail spars were cut from purchased carbon fiber tubes. All of the aerodynamic surfaces on the aircraft were 3D-printed. Polyethylene Terephthalate Glycol (PETG) was used as the material for the majority of the 3D-printed parts

for its combination of thermal resistance, impact strength, and reliability. Lightweight Polylactic Acid (LW-PLA) was used to print non-structural components including the control surfaces and fuselage component mounts due to its low density. The aerodynamic surfaces were printed in small sections and are designed to slide onto the spars. Clamps are installed on both ends of protruding spars to ensure that all pieces stay together firmly. Structural components were printed in PETG using different printing settings to optimize the strength to weight.

The carbon fiber tubes and rods used for booms and spars are purchased in 32-in and 72-in lengths respectively, and are cut into the required size. An extension piece is used for mounting the inboard front motors due to the length of the sized inboard booms exceeding 32 in. The main power cabling in the wing consists of 10 AWG cabling. The connections from the main bus are distributed using 12 AWG cabling to the lift motor ESCs and 10 AWG cabling to the cruise motor ESC. The complete manufactured version two of LPC-Lite is shown in Figure 10.

The servo motors are installed directly into pre-determined spots within the wing sections. There are two servos on either side of the wing, a single servo in each vertical tail, and a single servo in the horizontal tail. Together, these seven servos are responsible for actuating the flaperons, rudders, and elevators. Custom servo horns are installed on each servo along with a push-rod to actuate each control surface. The range of movement for each servo is independently controlled through parameters within QGroundControl and can be changed as required.

VII. Flight Test and Results

Initial flight tests for LPC-Lite occurred indoors within a netted facility at Auburn University. Following initial power-up and ground testing of control logic, the vehicle is placed on a pitch and roll rig. The rig is made by suspending a large carbon fiber rod between two wooden sawhorses. This carbon fiber rod passes directly through the fuselage, allowing the vehicle to rotate about a single axis in close proximity to the CG. The inner-loop LQI controllers are then tuned to ensure attitude command tracking and stability in each axis. For the yaw axis, the vehicle is attached to a spinning seat with low resistance, allowing the vehicle to spin freely about its yaw axis. Once all inner-loop controllers are tuned, the vehicle is then subjected to simple hop and hover tests within the net using a direct throttle and attitude control.

After several successful indoor flight tests, the testing moved outdoors to Sharpe Field in Tuskegee, AL (formerly a training base for the Tuskegee Airmen) for increased space to maneuver. Prior to flight tests, the simulation model is used to simulate the flight testing plan to catch any problems within the FCS. A total of three outdoor flight testing sessions have been made, with several more planned in the near future before the fly-off. The outdoor flight tests have provided useful insight for sensors and flight control law development. The flight testing has allowed for hover and low-speed transition (speeds at or below 30 mph) to be successfully tested. Forward flight mode has not been fully tested; however, upcoming flight tests are planned to focus on testing the entire flight envelope.

Autonomous flight testing is also planned for the upcoming flight tests. The autonomous flight has been verified in simulation testing and will be tested in simple point-to-point flight for initial testing, eventually becoming a full flight test course to prepare for the fly-off.

References

[1] Chakraborty, I., and Mishra, A. A., "Sizing and Analysis of a Lift-Plus-Cruise Aircraft with Electrified Propulsion," *Journal of Aircraft*, 2022, pp. 1–19.

[2] Comer, A. M., and Chakraborty, I., "Flight Control System Architecture for Urban Air Mobility Simplified Vehicle Operations," *AIAA SCITECH 2023 Forum*, 2023, p. 0399.

[3] Chakraborty, I., Comer, A. M., Bhandari, R., Mishra, A. A., Schaller, R., Sizoo, D., and McGuire, R., "Flight Simulation Based Assessment of Simplified Vehicle Operations for Urban Air Mobility," *AIAA SCITECH 2023 Forum*, 2023, p. 0400.

[4] Chakraborty, I., and Mishra, A. A., "Generalized Energy-Based Flight Vehicle Sizing and Performance Analysis Methodology," *Journal of Aircraft*, Vol. 58, No. 4, 2021, pp. 762–780.

[5] Chakraborty, I., Miller, N. S., and Mishra, A. A., "Sizing and Analysis of a Tilt-Wing Aircraft with All-Electric and Hybrid-Electric Propulsion Systems," *AIAA SCITECH 2022 Forum*, 2022, p. 1515.

[6] Drela, M., "QMIL user guide," *Propeller Analysis and Design URL: http://web. mit. edu/drela/Public/web/qprop*, 2005.

[7] Drela, M., "QPROP user guide," *Massachusetts Inst. of Technology Aeronautics and Astronautics, Cambridge, MA*, 2007.

[8] Comer, A., and Chakraborty, I., "Flight Control System Architecture for Urban Air Mobility Simplified Vehicle Operations," *AIAA SCITECH 2023 Forum*, AIAA-2023-0399, National Harbor, MD, 2023.

[9] Lambregts, A., "Integrated System Design for Flight and Propulsion Control Using Total Energy Principles," *AIAA Aircraft Design, Systems and Technology Meeting*, AIAA-83-2561, Fort Worth, TX, USA, Oct 17-19, 1983.

[10] Lambregts, A., "Functional Integration of Vertical Flight Path and Speed Control Using Energy Principles," *First Annual NASA Aircraft Controls Workshop*, NASA Langley Research Center, Hampton, VA, USA, Oct 25-27, 1983.

[11] Lambregts, A., "Vertical Flight Path and Speed Control Autopilot Design using Total Energy Principles," *AIAA Guidance and Control Conference*, AIAA-1983-2239, Gatlinburg, TN, USA, 15-17 August, 1983.

[12] Lambregts, A., "Operational Aspects of the Integrated Vertical Flight path and Speed Control System," *SAE Transactions*, Vol. 92, No. 4, 1983, pp. 29–41.

[13] MATLAB, *version 7.10.0 (R2022a)*, The MathWorks Inc., Natick, Massachusetts, 2022.